Estimation of Most Favorable Optical Window Position Subject to Achieve Finest Optical Control of Lateral DDR IMPATT Diode Designed to Operate at W-Band

Aritra ACHARYYA, Jayabrata GOSWAMI, Suranjana BANERJEE, J. P. BANERJEE

Institute of Radio Physics and Electronics, University of Calcutta, 92, APC Road, Kolkata 700009, India

ari_besu@yahoo.co.in, goswamijayabrata@gmail.com, suranjanarpe21@yahoo.com, jpbanerjee06@rediffmail.com

Abstract. *The optimum position of the optical window (OW) of illuminated lateral double-drift region (DDR) impact avalanche transit time (IMPATT) device has been determined subject to achieve the finest optical control of both DC and RF properties of the device. The OW is a tiny hole that has to be created on the oxide layer through which the light energy of appropriate wavelength can be coupled to the space charge region of the device. A non-sinusoidal voltage is assumed to be applied across the diode and the corresponding terminal current response is obtained from a two-dimensional (2-D) large-signal (L-S) simulation technique developed by the authors for illuminated lateral DDR IMPATT diode. Both the DC and L-S properties of the illuminated device based on Si, designed to operate at W-band frequencies (75–110 GHz) are obtained from the said L-S simulation. Simulation is carried out for different incident optical power levels of different wavelengths (600–1000 nm) by varying the position of the fixed sized OW on the oxide layer along the direction of electrical conduction of the device. Results show that, the most favorable optical tuning can be achieved when the OW is entirely created over the p-type depletion layer, i.e. when the photocurrent is purely electron dominated. Also the 700 nm wavelength is found to be most suitable wavelength for obtaining the maximum optical modulation of both DC and RF properties of the device.*

Keywords

Lateral DDR IMPATTs, finite difference method, optical window, W-band.

1. Introduction

Lateral Impact Avalanche Transit Time (IMPATT) structure has several inherent advantages over its conventional vertical counterpart. Some of those are ease of monolithic integration, series combination, coupling of light energy into the active region of the device to obtain better optical tuning of RF properties of the source, etc. In 1989, Stabile et al. [1] first reported two types of fabrication schemes of single-drift region (SDR) Si IMPATT diodes such as diffused and buried geometry. They also obtained suitable RF characteristics from both types of the diodes; although the buried structure was observed to provide better results. Later Attar et al. [2], [3] fabricated lateral SDR IMPATT diode, by using standard 0.18 μm complementary metal-oxide-semiconductor (CMOS) technology. They verified the RF performance of their fabricated device up to 77 GHz. In the year 2012, Acharyya et al. [4] first proposed a lateral double-drift region (DDR) Si IMPATT structure and intended a fabrication scheme for the same via standard CMOS technology. Later in the year 2013, the same authors reported a one-dimensional (1-D) small-signal (S-S) simulation technique to study the effect of photo-irradiation on the active region of the device [5]. They observed that under similar optical and electrical operating conditions, the better optical control of the RF properties of IMPATT devices may be achieved if the orientation of the device is lateral instead of vertical. But the above said simulation study is limited in accuracy and far from the practical operating condition due to the inherent limitations associated with the S-S simulation. Thus the large-signal (L-S) simulation is essential. The incident optical energy is vertically coupled with respect to the direction of electrical conduction through the device. Thus the two-dimensional (2-D) simulation is indispensible.

In this paper, the authors have presented a 2-D non-sinusoidal voltage excited (NSVE) L-S simulation technique to study the effect of optical illumination on the active region of lateral DDR IMPATT device. Different input optical power levels of different wavelengths (600 – 1000 nm) have been used in the present simulation. Both the DC and L-S properties of the illuminated device based on Si, designed to operate at W-band frequencies (75 to 110 GHz) are obtained from the said L-S simulation. The optimal position of the optical window (OW) on the SiO_2 layer (oxide layer) of the lateral DDR IMPATT is determined by shifting the OW from one edge of the depletion layer to another. Arrangement for optical illumination for three different OW positions are shown in Figs. 1 (a)–(c). The amount of changes in both DC and L-S properties of the device are observed for each position of the fixed sized OW. Finally the optimum position of the OW is deter-

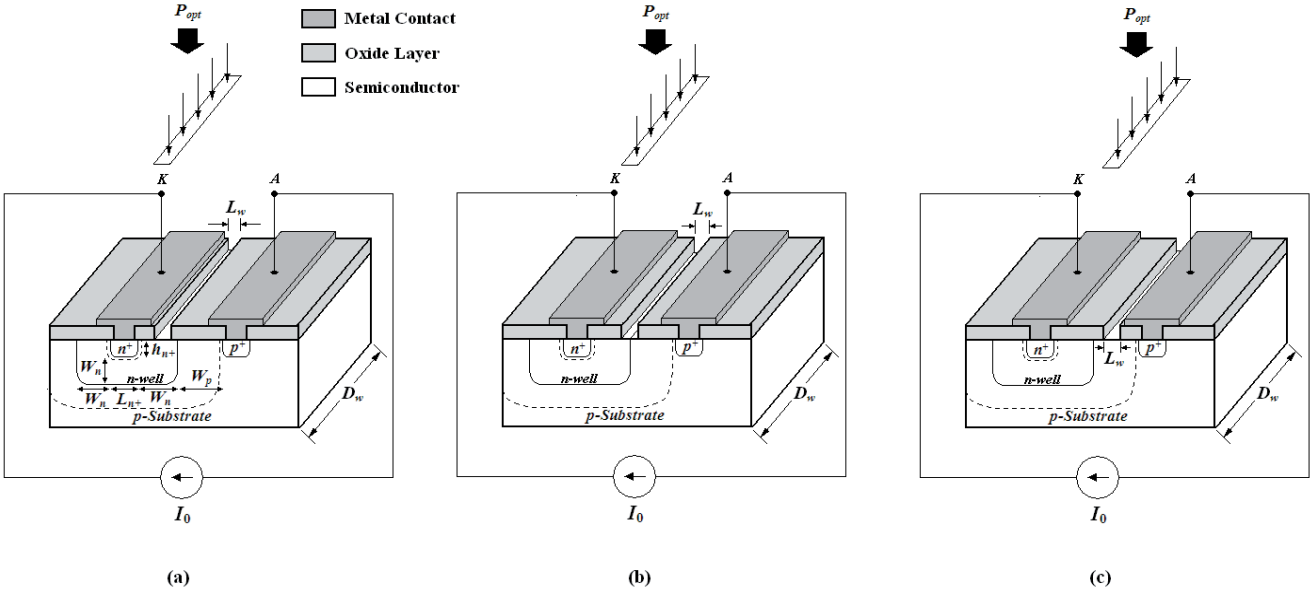

Fig. 1. Arrangement for optical illumination on different positions of space charge region such as **(a)** *n*-drift layer, **(b)** both *n*- and *p*-drift layers and **(c)** *p*-drift layer of reverse biased lateral DDR IMPATT through the OW of fixed illumination area ($A_w = L_w D_w$; where L_w and D_w are the length and width of the OW).

mined for which the above mentioned changes are maximum. It is observed that, the most favorable optical modulation of both DC and L-S properties of the device can be achieved when the OW is entirely placed over the *p*-drift layer, i.e. when the generated photocurrent is completely electron dominated. It is also observed that the most favorable wavelength for which the maximum optical modulation can be achieved is 700 nm, which is nearly the wavelength corresponding to the peak responsivity of Si, i.e. 750 nm.

2. Design and Material Parameters

The 2-D model of the lateral DDR IMPATT diode is shown in Fig. 2. In the present simulation method, the cross-sectional shape of the metallurgical junction is taken to be rectangular, though the actual shape of the same is different as shown in Figs. 1 (a)–(c). In the lateral DDR IMPATTs, the light energy is coupled along the *y*-axis with the active region of the device. However the direction of current conduction through the device is along *x*-axis. Thus the study of cross-coupling of light energy with the electrical conduction of the device is important. That is why, in the present modeling, the actual cross-sectional shape of the metallurgical junction and thus that of the depletion layer (which are less important) are not taken into account. The widths of the *n*- and *p*-epitaxial layers (W_n, W_p), corresponding doping concentrations (N_D, N_A respectively), widths of highly doped n^+- and p^+-layers (W_{n+}, W_{p+}) and corresponding doping concentrations (N_{n+}, N_{p+} respectively) are chosen initially by using the transit time formula of Sze and Ryder [6] for operation at W-band and finally optimized subject to obtain maximum DC to RF conversion efficiency by using the 2-D NSVE L-S simulation method discussed in the next section. Again the bias current density (J_0) parameter is also optimized subject to obtain the maximum DC to RF conversion efficiency of the device at W-band frequencies. The effective *n*-*p* metallurgical junction area of the device is taken to be $A_j = 10^9\ \mathrm{m}^{-2}$ which is suitable for W-band operation [7]. The structural, doping and bias current density parameters of the designed device are given in Tab. 1.

Design parameters	Values
W_n (μm)	0.400
W_p (μm)	0.380
N_D ($\times 10^{23}$ m^{-3})	1.200
N_A ($\times 10^{23}$ m^{-3})	1.250
N_{n+} ($\times 10^{25}$ m^{-3})	5.000
N_{p+} ($\times 10^{25}$ m^{-3})	2.700
J_0 ($\times 10^8$ A m^{-2})	3.400
A_j (m^{-2})	10^9

Tab. 1. Structural, doping and other parameters.

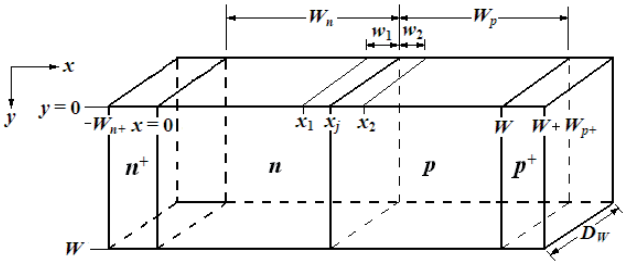

Fig. 2. 2-D model of the lateral DDR (n^+-*n*-*p*-p^+) IMPATT diode ($w_1 = w_2 = 0.1$ μm).

The 2-D doping profile of the device may be formulated as

$$N(x,y)=\begin{cases} N_{n^+}\exp\left(-1.08\lambda_n(x)-0.78\lambda_n(x)^2\right) & x\le 0 \\ =N_D & 0<x\le x_1 \\ =N_D\left[1-\exp(x/s)\right] & x_1<x\le x_j \\ =-N_A\left[\exp(-x/s)-1\right] & x_j<x\le x_2 \\ =-N_A & x_2<x<W \\ =-N_{p^+}\exp\left(-1.08\lambda_p(x)-0.78\lambda_p(x)^2\right) & x\ge W \end{cases} \Bigg\} 0\le y\le W \quad (1)$$

where $\lambda_n(x)=\left(W_{n^+}+x\right)\big/2\sqrt{(Dt_d)}$ and $\lambda_p(x)=\left(W_{p^+}+x-W\right)\big/2\sqrt{(Dt_d)}$ (D is the impurity diffusion constant, t_d is the time for diffusion), s is a constant whose value may be taken as ≈ 5 nm and the value of the Dt_d is taken to be 4.0×10^{-12} m^2 and W is the total depletion layer width ($W = W_n + W_p$). Here the doping profile near the n-p metallurgical junction (i.e. within $x_1 < x \le x_2$) is approximated by incorporating an appropriate exponential function. While the doping profiles near the n-n^+ and p-p^+ interfaces (i.e. $x \le 0$ and $x \ge W$ respectively) are taken into account by an equivalent complementary error function [8]. The 2-D plot of the doping profile of the designed W-band lateral DDR Si IMPATT diode is shown in Fig. 3 which is taken as one of the inputs in the 2-D NSVE- L-S simulation described in the next section.

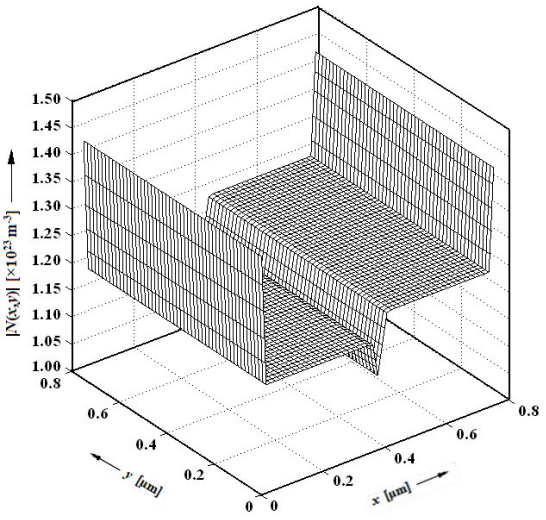

Fig. 3. 2-D doping profile within the epitaxial region of the lateral DDR Si IMPATT diode design to operate at W-band (2-D 70×70 grids).

The electronic material parameters of Si such as electric field dependent ionization rates (α_n, α_p) and drift velocities (v_n, v_p) of charge carriers, bandgap (E_g), intrinsic carrier concentration (n_i), effective density of states of conduction and valance bands (N_c, N_v), effective mass of electrons in conduction band (m_n^*) and that of holes in valance band (m_p^*), density of state effective mass of charge carriers (m_d^*), mobility of electrons and holes (μ_n, μ_p), diffusion coefficients (D_n, D_p), diffusion lengths (L_n, L_p), etc. at realistic junction temperature of T_j = 500 K are taken from published experimental reports [9-11]. The optoelectronic parameters of Si such as absorption coefficient ($\alpha(\lambda)$), refractive index ($n_s(\lambda)$), internal quantum efficiency ($\eta_{int}(\lambda)$), etc. at the wavelengths under consideration (i.e. 600–1000 nm) at 500 K are taken from recently published experimental reports [12-14].

3. The Proposed Model and Simulation Technique

The 2-D model of the lateral DDR (n^+-n-p-p^+) IMPATT structure shown in Fig. 4 is used for the present simulation study. Initial position of the OW is defined from $x = x_{ws0}$ to $x = x_{we0}$ as shown in Fig. 4 (a). Each time, the OW is shifted along the positive x-direction by a small length Δx and both the DC and L-S parameters of the device are obtained from the simulation for a particular input optical power (P_{opt}) of wavelength λ. The final position of the starting edge of the OW is $x = x_{wsf}$. Thus the value of Δx may be obtained from $\Delta x = (x_{wsf} - x_{ws0})/n$; where the value of n is taken to be 50 in the present simulation. Figs. 4 (a)–(d) show the different OW positions along the positive x-axis. The final position of the OW (i.e. $x = x_{wsf}$) is chosen by keeping in mind $(W - x_{wsf}) \le L_w$.

If the optical power P_{opt} of wavelength λ is assumed to be incident on the device through the OW, then for any position of the OW, the surface density of the photon flux is given by $\Phi_0(\lambda)=P_{opt}\left(1-R'(\lambda)\right)\lambda/A_w hc$, where $R'(\lambda)$ is the reflectance of the semiconductor-air interface ($R'(\lambda)$ = $(n_s(\lambda) - n_a(\lambda))/ (n_s(\lambda) + n_a(\lambda))$; where $n_s(\lambda)$ and $n_a(\lambda)$ are the refractive index of the semiconductor and air respectively at wavelength λ), A_w is the illumination area ($A_w = L_w D_w$; L_w and D_w are the length ($L_w < W_n$ and $L_w < W_p$) and width of the OW as shown in Figs. 4 (a)–(d)), h is the Planck's constant ($h = 6.625\times10^{-34}$ J s) and c is the velocity of light in free space ($c = 3.0\times10^8$ ms^{-1}). At any position of the OW along the positive x-axis, the electron-hole pair (EHP) generation rate due to optical illumination of wavelength λ is given by $G_L^{(\lambda)}(y)=\eta_{\text{int}}(\lambda)\alpha(\lambda)\Phi_0(\lambda)\exp(-\alpha(\lambda)y)$ for $x_{ws}^{(i)}(x) \le x \le x_{we}^{(i)}(x)$ and $0 \le y \le W$, where $\eta_{int}(\lambda)$ and $\alpha(\lambda)$ are the internal quantum efficiency (number of EHP generated per photon) and absorption coefficient of the semiconductor material respectively at wavelength λ, $x_{ws}^{(i)}(x)$ and $x_{we}^{(i)}(x)$ are the coordinates of the starting and ending edges of the OW respectively along the positive x-axis. The starting and ending coordinates of the OW for i^{th} position of it may be formulated as $x_{ws}^{(i)}(x) = (x_{ws0} + i\Delta x)$ and $x_{we}^{(i)}(x) = (x_{we0} + i\Delta x)$; where i is any integer having range $0 \le i \le n$. The EHP generation rate at any spatial position (x,y) is independent of x-coordinate, since the constant photon flux density (which is independent of x-coordinate) is assumed to incident on the depletion layer of the device through the OW. Now the electron and hole dominated photocurrent densities may be calculated as follows.

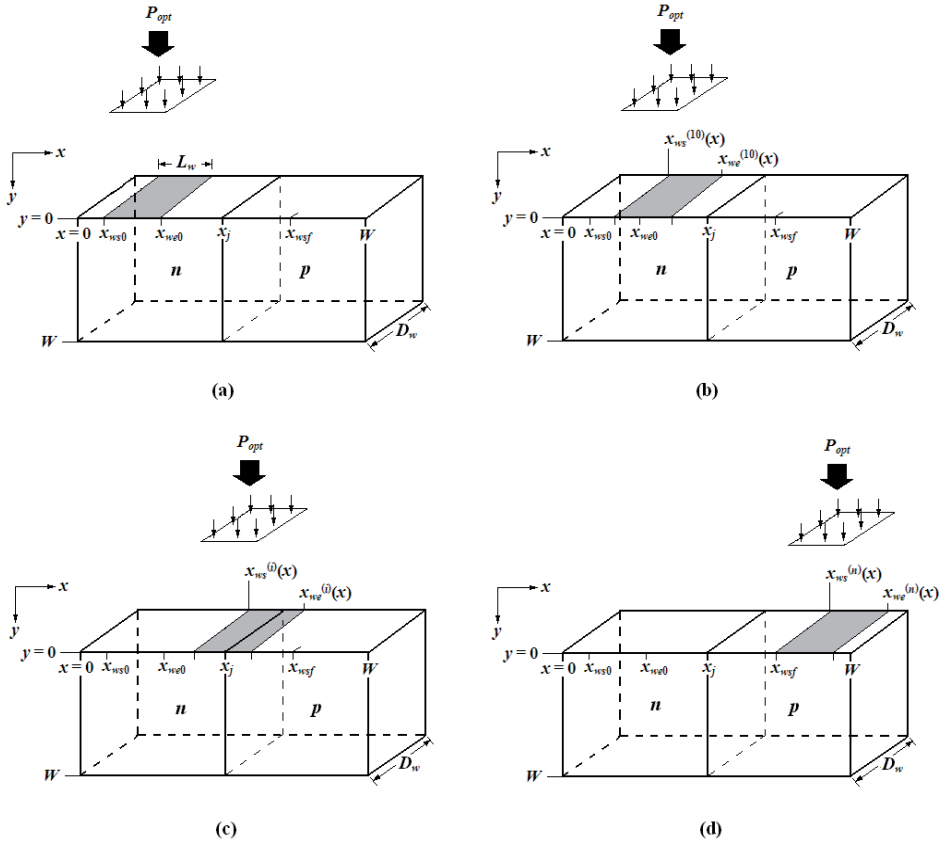

Fig. 4. 2-D model of the lateral DDR IMPATT diode showing different positions of the OW: **(a)** initial position, i.e. from $x = x_{ws0}$ to $x = x_{we0}$, **(b)** 10th intermediate position, i.e. from $x = (x_{ws0} + 10\Delta x)$ to $x = (x_{we0} + 10\Delta x)$, **(c)** i^{th} intermediate position, i.e. from $x = (x_{ws0} + i\Delta x)$ to $x = (x_{we0} + i\Delta x)$ and **(d)** final position, i.e. from $x = (x_{ws0} + n\Delta x)$ to $x = (x_{we0} + n\Delta x)$.

3.1 Photocurrent Densities

When the light is incident on the *n*-drift layer of the device (i.e. when $x_{we}^{(i)}(x) \le x_j$; where x_j is the position of the metallurgical junction), then the photocurrent density becomes purely hole dominated; similarly when the light is incident on the *p*-drift layer of the device (i.e. when $x_{ws}^{(i)}(x) \ge x_j$), then the photocurrent density becomes purely electron dominated [5]. But when the light is allowed to incident simultaneously on both *n*- and *p*-drift layers (i.e. when $x_{ws}^{(i)}(x) < x_j$ and $x_{we}^{(i)}(x) > x_j$), then both the electron and hole dominated photocurrent densities are generated concurrently. The drift component of hole dominated photocurrent density for a given input optical power (P_{opt}) of wavelength λ for i^{th} position of the OW can be expressed as

$$J_{h^+(opt\_drt)}^{(\lambda,i)}(x,y) = q\int_0^{l_n^{(i)}(x)} G_L^{(\lambda)}(y)dx = q\eta_{\text{int}}(\lambda)\alpha(\lambda)\Phi_0(\lambda)\exp(-\alpha(\lambda)y)l_n^{(i)}(x)$$
$$\text{for } 0 \le x \le W \text{ and } 0 \le y \le W. \quad (2)$$

Similarly the drift component of electron dominated photocurrent density for a given input optical power (P_{opt}) of wavelength λ for i^{th} position of the OW can be expressed as

$$J_{e^-(opt\_drt)}^{(\lambda,i)}(x,y) = q\int_0^{l_p^{(i)}(x)} G_L^{(\lambda)}(y)dx = q\eta_{\text{int}}(\lambda)\alpha(\lambda)\Phi_0(\lambda)\exp(-\alpha(\lambda)y)l_p^{(i)}(x)$$
$$\text{for } 0 \le x \le W \text{ and } 0 \le y \le W. \quad (3)$$

The parameters $l_n^{(i)}(x)$ and $l_p^{(i)}(x)$ in (2) and (3) are the effective lengths of the OW over the *n*- and *p*-drift layers respectively. These effective lengths ($l_n^{(i)}(x)$ and $l_p^{(i)}(x)$) may be formulated in terms of the starting and ending coordinates of the OW ($x_{ws}^{(i)}(x)$ and $x_{we}^{(i)}(x)$) for any position of it (i.e. for any integer value of i within the range $0 \le i \le n$) and the position of the metallurgical junction (i.e. $x = x_j$); those are given by

$$l_n^{(i)}(x) = \left(x_{we}^{(i)}(x) - x_{ws}^{(i)}(x)\right) = L_w \quad \text{for } x_{we}^{(i)}(x) \le x_j,$$
$$= \left(x_j - x_{ws}^{(i)}(x)\right) \quad \text{for } x_{ws}^{(i)}(x) < x_j \text{ and } x_{we}^{(i)}(x) > x_j,$$
$$= 0 \quad \text{for } x_{ws}^{(i)}(x) \ge x_j, \quad (4)$$

$$l_p^{(i)}(x) = 0 \quad \text{for } x_{we}^{(i)}(x) \le x_j$$
$$= \left(x_j - x_{ws}^{(i)}(x)\right) \quad \text{for } x_{ws}^{(i)}(x) < x_j \text{ and } x_{we}^{(i)}(x) > x_j,$$
$$= \left(x_{we}^{(i)}(x) - x_{ws}^{(i)}(x)\right) = L_w \quad \text{for } x_{ws}^{(i)}(x) \ge x_j \quad (5)$$

Due to the absence of electric field in both highly doped and undepleted n^+-and p^+-layers, current flow occur within those layers via diffusion mechanism. The diffusion components of photocurrent densities within n^+-and p^+-layers are obtained by solving the 2-D ambipolar transport equations subject to appropriate boundary conditions. The solutions are given by

$$J^{(\lambda)}_{h^+(opt\_dff)}(y)=q\eta_{\text{int}}(\lambda)\Phi_0(\lambda)\left(\frac{\alpha(\lambda)L_p}{1+\alpha(\lambda)L_p}\right)\exp(-\alpha(\lambda)y), \quad (6)$$

$$J^{(\lambda)}_{e^-(opt\_dff)}(y)=q\eta_{\text{int}}(\lambda)\Phi_0(\lambda)\left(\frac{\alpha(\lambda)L_n}{1+\alpha(\lambda)L_n}\right)\exp(-\alpha(\lambda)y). \quad (7)$$

The total electron and hole dominated photocurrent densities may be obtained as the combination of respective drift and diffusion components. Thus

$$J^{(\lambda,i)}_{h^+(opt)}(x,y)=J^{(\lambda,i)}_{h^+(opt\_drt)}(x,y)+J^{(\lambda)}_{h^+(opt\_dff)}(y), \quad (8)$$

$$J^{(\lambda,i)}_{e^-(opt)}(x,y)=J^{(\lambda,i)}_{e^-(opt\_drt)}(x,y)+J^{(\lambda)}_{e^-(opt\_dff)}(y). \quad (9)$$

3.2 2-D L-S Simulation Technique

Both DC and L-S properties of illuminated lateral DDR IMPATT diode has been studied by varying the position of the OW for different incident optical power (P_{opt}) of wavelength λ by using a 2-D NSVE L-S simulation method. The fundamental time and space (2-D) dependent device equations such as Poisson's equation (10), continuity equations involving both avalanche and band to band tunneling generation rates ((11) and (12)) and current density equations ((13) and (14)) are simultaneously solved subject to appropriate time dependent boundary conditions under both dark ($P_{opt}=0$) and different illuminated conditions (i.e. for finite P_{opt} of wavelength λ) for different OW positions. The design parameters (W_n, W_p, N_D, N_A, N_{n+}, N_{p+}, D_j), doping profile (Fig. 3), bias current density (J_0) and material parameters of the base semiconductor are taken as the inputs of simulation. The time and space dependent fundamental device equations are given by

$$\nabla^2 V^{(\lambda,i)}(x,y,t)=-\frac{q}{\varepsilon_s}\left(N(x,y)+p^{(\lambda,i)}(x,y,t)-n^{(\lambda,i)}(x,y,t)\right), \quad (10)$$

$$\frac{\partial p^{(\lambda,i)}(x,y,t)}{\partial t}=\left(-\frac{1}{q}\right)\nabla J^{(\lambda,i)}_{h^+(tot)}(x,y,t)+G^{(\lambda,i)}_{Ah^+}(x,y,t)+G^{(\lambda,i)}_{Th^+}(x,y,t), \quad (11)$$

$$\frac{\partial n^{(\lambda,i)}(x,y,t)}{\partial t}=\left(\frac{1}{q}\right)\nabla J^{(\lambda,i)}_{e^-(tot)}(x,y,t)+G^{(\lambda,i)}_{Ae^-}(x,y,t)+G^{(\lambda,i)}_{Te^-}(x,y,t), \quad (12)$$

$$J^{(\lambda,i)}_{h^+(tot)}(x,y,t)=-q\begin{bmatrix}\mu_p p^{(\lambda,i)}(x,y,t)\nabla V^{(\lambda,i)}(x,y,t)\\+D_p\nabla p^{(\lambda,i)}(x,y,t)\end{bmatrix}+J^{(\lambda,i)}_{h^+(opt)}(x,y,t), \quad (13)$$

$$J^{(\lambda,i)}_{e^-(tot)}(x,y,t)=-q\begin{bmatrix}\mu_n n^{(\lambda,i)}(x,y,t)\nabla V^{(\lambda,i)}(x,y,t)\\-D_n\nabla n^{(\lambda,i)}(x,y,t)\end{bmatrix}+J^{(\lambda,i)}_{e^-(opt)}(x,y,t), \quad (14)$$

where $V^{(\lambda,i)}(x,y,t)$, $p^{(\lambda,i)}(x,y,t)$, $n^{(\lambda,i)}(x,y,t)$, $J^{(\lambda,i)}_{h^+(tot)}(x,y,t)$ and $J^{(\lambda,i)}_{e^-(tot)}(x,y,t)$ are the electric potential, hole and electron concentrations, total hole and electron components of current densities respectively at any space point (x,y) within the space charge layer at the time instant t within the fundamental time period of the steady-state oscillation, under illuminated condition for a particular positions of the OW, ε_s is the permittivity of the semiconductor material, q is the unit electronic charge ($q = 1.6\times10^{-19}$ C). The electric field at any space point (x,y) within the depletion layer at the time instant t within the fundamental time period of the steady-state oscillation can be obtained from $\xi^{(\lambda,i)}(x,y,t)=-\nabla V^{(\lambda,i)}(x,y,t)$. The recombination effects are not included in the current continuity equations ((11) and (12)), since the transit time of charge carriers in the depletion layer of an IMPATT diode is several order of magnitude shorter than the recombination time. The avalanche generation rates of electrons and holes at any space point (x,y) at the time instant t are given by

$$G^{(\lambda,i)}_{Ae^-}(x,y,t)=G^{(\lambda,i)}_{Ah^+}(x,y,t)=n^{(\lambda,i)}(x,y,t)\alpha^{(\lambda,i)}_n(x,y,t)v^{(\lambda,i)}_n(x,y,t)+p^{(\lambda,i)}(x,y,t)\alpha^{(\lambda,i)}_p(x,y,t)v^{(\lambda,i)}_p(x,y,t), \quad (15)$$

where $\alpha^{(\lambda,i)}_n(x,y,t)$ and $\alpha^{(\lambda,i)}_p(x,y,t)$ are the ionization rates and $v^{(\lambda,i)}_n(x,y,t)$ and $v^{(\lambda,i)}_p(x,y,t)$ are the drift velocities of electrons and holes respectively at (x,y) at the instant of time t. The tunneling generation rate for electrons at the space point (x,y) at the instant of time t may be calculated by quantum mechanical considerations [15] and may be written as

$$G^{(\lambda,i)}_{Te^-}(x,y,t)=a_T\left(\xi^{(\lambda,i)}(x,y,t)\right)^2\exp\left(-\frac{b_T}{\xi^{(\lambda,i)}(x,y,t)}\right), \quad (16)$$

where the coefficients a_T and b_T are

$$a_T=\frac{q^2}{8\pi^3\hbar^2}\left(\frac{2m_d{}^*}{E_g}\right)^{\frac{1}{2}} \text{ and } b_T=\frac{1}{2q\hbar}\left(\frac{m_d{}^*E_g{}^3}{2}\right)^{\frac{1}{2}}. \quad (17)$$

In the above equations, $m_d{}^*$ is the density of state elective mass of charge carriers, E_g is the bandgap of the semiconductor and the normalized Planck's constant is given by $\hbar = h/2\pi$. The tunneling generation rate for holes can be obtained from 2-D version of the earlier reported 1-D energy-band diagram of reverse biased DDR IMPATT [16], [17]. The phenomenon of tunneling is instantaneous and the tunnel generation rate for holes at (x,y) at instant of time t is equal to that for electrons at some other space point (x',y) at the same instant of time t, i.e.

$G_{Th^+}^{(\lambda,i)}(x,y,t)=G_{Te^-}^{(\lambda,i)}(x',y,t)$. The tunnel generation of an electron at (x',y) is simultaneously associated with the generation of a hole at (x,y), where $(x-x')$ is the spatial separation between the edge of conduction band and valence band at the same energy. If E is the measure of energy from the bottom of the conduction band on the n-side and the vertical difference between (x,y) and (x',y) is E_g, x' can be easily obtained from [16], [17]

$$x=x'\left(1-\frac{E_g}{E}\right)^{-\frac{1}{2}} \quad \text{for } 0\le x\le x_j,\ 0\le y\le W \qquad (18)$$

$$x=W-\left(W-x'\right)\left(1+\frac{E_g}{E_B-E}\right)^{-\frac{1}{2}} \quad \text{for } x_j\le x\le W,\ 0\le y\le W. \qquad (19)$$

The time varying boundary conditions for the electric field at the depletion layer edges, i.e. at $x = 0$ and $x = W$, $0 \le y \le W$ are given by

$$\xi^{(\lambda,i)}(x=0,y,t)=\xi^{(\lambda,i)}(x=W,y,t)=0 \quad \text{for } 0\le y\le W. \qquad (20)$$

Similarly the time varying boundary conditions for the normalized current density (i.e. $P^{(\lambda,i)}(x,y,t)=\left[J_{h^+(tot)}^{(\lambda,i)}(x,y,t)-J_{e^-(tot)}^{(\lambda,i)}(x,y,t)\right]/J_t^{(\lambda,i)}(x,y,t)$; where $J_t^{(\lambda,i)}(x,y,t)=J_{h^+(tot)}^{(\lambda,i)}(x,y,t)+J_{e^-(tot)}^{(\lambda,i)}(x,y,t)$) at the depletion layer edges, i.e. at $x = 0$ and $x = W$, $0 \le y \le W$ are given by

$$\left.\begin{aligned}P^{(\lambda,i)}(x=0,y,t)&=\left(\frac{2J_{h^+(tot)}^{(\lambda,i)}(x=0,y,t)}{J_t^{(\lambda,i)}(x=0,y,t)}-1\right),\\ P^{(\lambda,i)}(x=W,y,t)&=\left(1-\frac{2J_{e^-(tot)}^{(\lambda,i)}(x=W,y,t)}{J_t^{(\lambda,i)}(x=W,y,t)}\right)\end{aligned}\right\} \quad \text{for } 0\le y\le W. \qquad (21)$$

Along the floating boundaries, i.e. at $y = 0$ and $y = W$, $0 \le x \le W$ the current boundary conditions are taken as

$$J_{h^+(tot)}^{(\lambda,i)}(x,y=0,t)=J_{e^-(tot)}^{(\lambda,i)}(x,y=0,t)=0$$

and $$J_{h^+(tot)}^{(\lambda,i)}(x,y=W,t)=J_{e^-(tot)}^{(\lambda,i)}(x,y=W,t)=0\,. \qquad (22)$$

As for the space charge boundary conditions along the floating boundaries, i.e. at $y = 0$ and $y = W$, $0 \le x \le W$ the following conditions are adopted

$$\frac{\partial}{\partial x}\left(N(x,y=0)+p^{(\lambda,i)}(x,y=0,t)-n^{(\lambda,i)}(x,y=0,t)\right)=0 \quad \text{and}$$

$$\frac{\partial}{\partial x}\left(N(x,y=W)+p^{(\lambda,i)}(x,y=W,t)-n^{(\lambda,i)}(x,y=W,t)\right)=0\,. \qquad (23)$$

Equation (23) is less restrictive than the condition of zero space charge variation proposed by Kurata [22]. The choice of (23) is required because of the asymmetry introduced in the present problem by the incident optical power.

In the present method, a non-sinusoidal voltage excitation (NSVE) model have been adopted where a non-sinusoidal voltage ($v_{rf}(t)$) having form $v_{rf}(t)=V_B\sum_{p=1}^{m}m_x{}^p\sin(2p\pi f_d t)$, with fundamental frequency f_d and $(m-1)$ harmonics is assumed to be applied across the IMPATT device through a coupling capacitor (C) as shown in Fig. 5. The consequent current response of the device (which is biased with the DC current $I_0 = J_0 A_j$; where A_j is the effective junction area of the device) is obtained by simultaneously solving equations (10) – (14) subject to boundary conditions given in equations (20) – (23). The voltage modulation factor (m_x) is the measure of the amount of RF voltage swing over the DC breakdown voltage (V_B) across the device under dark condition. Thus the fundamental component of RF voltage may be written as $v_{rf1}(t) = m_x V_B \sin(2\pi f_d t)$. The total photocurrent in illuminated device is represented by the photocurrent source $\left(I_{(opt)}^{(\lambda,i)}=A_j\int_{x=0}^{W}\int_{y=0}^{W}\left(J_{h^+(opt)}^{(\lambda,i)}(x,y)+J_{e^-(opt)}^{(\lambda,i)}(x,y)\right)dx\,dy\right)$ in parallel with the bias current source (I_0) as shown in Fig. 5. At first, the DC simulation is carried out by keeping the entire simulation technique time independent. The 2-D spatial distributions of the DC electric field ($\xi^{(\lambda,i)}(x,y)$ vs. x vs. y), electric potential ($V^{(\lambda,i)}(x,y)$ vs. x vs. y), electron and hole components of total current densities ($J_{e^-(tot)}^{(\lambda,i)}(x,y)$ and $J_{h^+(tot)}^{(\lambda,i)}(x,y)$ vs. x vs. y) within the depletion layer of the device are obtained from the simultaneous numerical solution of the time independent and space dependent fundamental device equations subject to appropriate time independent boundary conditions for a particular incident optical power (P_{opt}) of wavelength λ for a particular position of the OW. The DC breakdown voltage of the device for a particular incident optical power (P_{opt}) of wavelength λ for a particular position of the OW may be obtained as $V_B^{(\lambda,i)}=-\int_{x=0}^{W}\int_{y=0}^{W}\xi^{(\lambda,i)}(x,y)dx\,dy$.

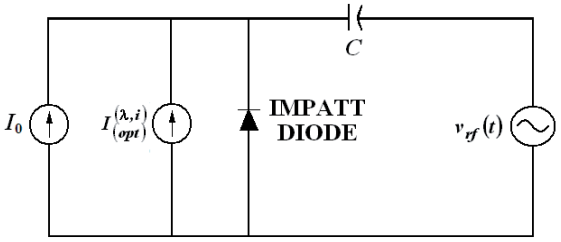

Fig. 5. Equivalent circuit of voltage driven IMPATT oscillator under optical illumination.

After obtaining $V_B^{(\lambda,i)}$, the RF voltage ($v_{rf}(t)$) introduces the time dependence into the simulation by introducing time varying voltage $V^{(\lambda,i)}(x,y,t)=V^{(\lambda,i)}(x,y)+v_{rf}(t)$ in place of time independent $V^{(\lambda,i)}(x,y)$. The snap-shots of electric field ($\xi^{(\lambda,i)}(x,y,t)$ vs. x vs. y at t), electric potential ($V^{(\lambda,i)}(x,y,t)$ vs. x vs. y at t), electron and hole components of total current densities ($J_{e^-(tot)}^{(\lambda,i)}(x,y,t)$ and $J_{h^+(tot)}^{(\lambda,i)}(x,y,t)$ vs. x vs. y at t) within the depletion layer of the device are

obtained from the simultaneous numerical solution of the time and space dependent fundamental device equations (10)–(14) subject to appropriate time dependent boundary conditions (20)–(23) at different time instants (i.e. t; $rT_d \le t \le (r+1)T_d$, where $r = 0, 1, 2, 3, \ldots\ldots$) of the fundamental time period of the steady-state oscillation ($T_d = 1/f_d$) for a particular incident optical power (P_{opt}) of wavelength λ for a particular position of the OW. In the present technique, 2-D finite difference method (FDM) with 70×70 spatial grids along with 50 time steps is used to obtain the numerical solution of the above mentioned simultaneous differential equations with sufficient accuracy. The instantaneous diode terminal voltage for a particular incident optical power (P_{opt}) of wavelength λ for the i^{th} position of the OW may be calculated as $V_t^{(\lambda,i)}(t) = -\int_{x=0}^{W}\int_{y=0}^{W}\xi^{(\lambda,i)}(x,y,t)\,dx\,dy$. The L-S program is run until the limit of one complete cycle (i.e. $0 \le \omega_d t \le 2\pi$) is reached. However, initially few cycles are repeated to confirm the stability of oscillation. Once the stability is reached, the instantaneous diode terminal voltage ($V_t^{(\lambda,i)}(t)$) and corresponding current response ($J_t^{(\lambda,i)}(t) = \int_{x=0}^{W}\int_{y=0}^{W}\left(J_{h^+(tot)}^{(\lambda,i)}(x,y,t) + J_{e^-(tot)}^{(\lambda,i)}(x,y,t)\right)dx\,dy$) are Fourier transformed to obtain the frequency domain information of those. Then the terminal current is divided by the terminal voltage (both in frequency domain) to obtain the L-S device admittance ($Y_D^{(\lambda,i)}(f)$) as a function of frequency (f). The L-S device admittance ($Y_D^{(\lambda,i)}(f) = G^{(\lambda,i)}(f) + jB^{(\lambda,i)}(f)$) is then resolved to real and imaginary parts to obtain L-S negative conductance ($G^{(\lambda,i)}(f)$) and corresponding susceptance ($B^{(\lambda,i)}(f)$) as functions of frequency. Thus the admittance characteristics (i.e. $G^{(\lambda,i)}(f)$ vs. $B^{(\lambda,i)}(f)$ plot) for a bias current density (J_0), incident optical power (P_{opt}) of wavelength λ for a particular position of the OW can be obtained from the above mentioned procedure.

From the L-S admittance characteristics, several important L-S parameters of the device such as optimum frequency ($f_p^{(\lambda,i)}$), avalanche resonance frequency ($f_a^{(\lambda,i)}$), peak negative conductance ($G_p^{(\lambda,i)}$), corresponding susceptance ($B_p^{(\lambda,i)}$), negative resistance ($Z_R^{(\lambda,i)}(f)$), reactance ($Z_X^{(\lambda,i)}(f)$) and Q-factor ($Q_p^{(\lambda,i)} = -\left(B_p^{(\lambda,i)}/G_p^{(\lambda,i)}\right)$), etc. may be obtained. Now the fundamental component of the L-S RF power output ($P_{RF}^{(\lambda,i)}$) may be calculated as $P_{RF}^{(\lambda,i)} = \frac{1}{2}V_{RF1}^{(\lambda,i)2}\left|G_p^{(\lambda,i)}\right|A_j$, where $V_{RF1}^{(\lambda,i)}$ is the amplitude of the RF voltage ($V_{RF1}^{(\lambda,i)} = m_x V_B^{(\lambda,i)}$), $|G_p^{(\lambda,i)}|$ is the magnitude of L-S peak negative conductance normalized with respect to effective junction area (A_j). The fundamental component of the L-S DC to RF conversion efficiency ($\eta_L^{(\lambda,i)}$) of the device is obtained from $\eta_L^{(\lambda,i)} = \left(P_{RF}^{(\lambda,i)}/P_{DC}^{(\lambda,i)}\right)$, where $P_{DC}^{(\lambda,i)} = J_0 V_B^{(\lambda,i)} A_j$ is the input DC power. Thus by using the present simulation method, both the static (DC) and L-S characteristics of the lateral DDR IMPATT device designed to operate at a particular frequency can be obtained for different incident optical power (P_{opt}) of wavelength λ for a particular position of the OW. Once the simulation is completed for a particular position of the OW, the new position of the OW is defined by increasing the parameter 'i' as per the formulation presented in this paper. Ultimately, the DC and L-S properties of the device may be investigated for different P_{opt} of different λ by shifting the OW from its initial position defined by $i = 0$ (i.e. $x_{ws}^{(i)}(x) = x_{ws0}$) to its final position defined by $i = n$ (i.e. $x_{ws}^{(i)}(x) = x_{wsf}$). Thus total ($n + 1$) sets DC and L-S results are available for each set of J_0, P_{opt} and λ. From those results the optimum position of the OW is obtained for which the maximum optical modulation of the DC and L-S properties of the device have been achieved.

4. Results and Discussion

In this section, the DC and L-S properties of the lateral DDR Si IMPATT device designed to operate at W-band under dark and illuminated conditions are presented. The above mentioned characteristics of the device are obtained for different positions of the starting of the OW along x-direction from $x_{ws0} = 0.01$ μm to $x_{wsf} = 0.58$ μm.

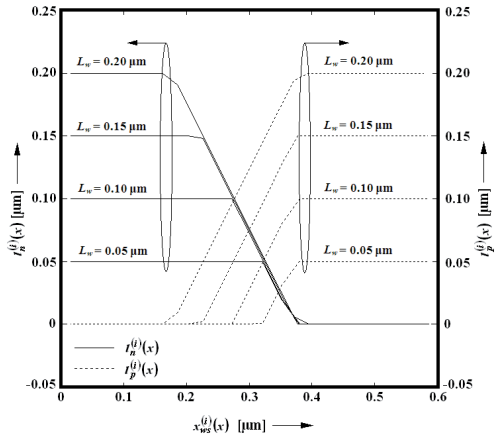

Fig. 6. Variations of effective n-side and p-side OW lengths ($l_n^{(i)}(x)$ and $l_p^{(i)}(x)$) for different physical lengths of the same (L_w) with the starting position of the optical window ($x_{ws}^{(i)}(x)$) along the length of the depletion layer (x-direction).

Variations of effective n-side and p-side OW lengths ($l_n^{(i)}(x)$ and $l_p^{(i)}(x)$) for different physical lengths of the same (L_w) with the starting position of the optical window ($x_{ws}^{(i)}(x)$) along the length of the depletion layer (x-direction) are shown in Fig. 6 (equations (4) and (5)). Finally the physical size of the OW is chosen to be $L_w = 0.20$ μm for the present simulation study, keeping in mind the tech-

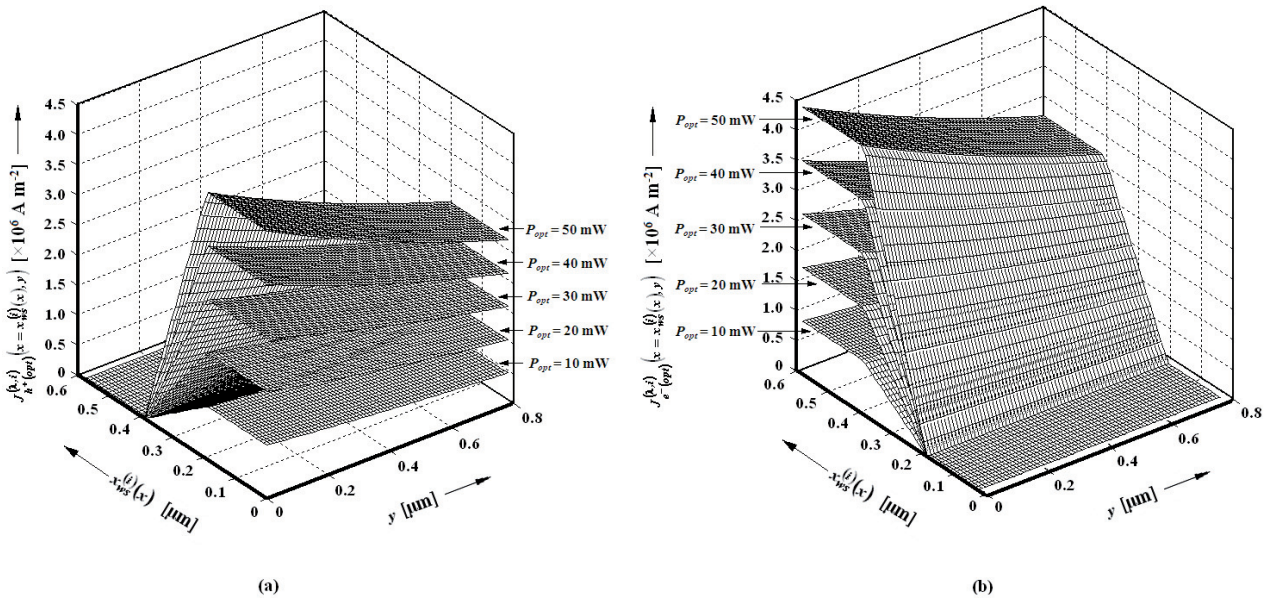

Fig. 7. Variations of **(a)** hole and **(b)** electron dominated photocurrent densities with the depth of the depletion layer (y-direction) and starting position of the OW along the length of the depletion layer (x-direction) for different incident optical power (P_{opt}) of wavelength λ = 700 nm (OW size: L_w = 0.20 μm, D_w = 0.40 mm, illumination area $A_w = L_w D_w = 0.80\times10^{-10}$ m^2) (2-D FDM: 50×70 grids).

nological feasibility. Variations of hole and electron dominated photocurrent densities with the depth of the depletion layer (y-direction) and starting position of the OW along the length of the depletion layer (x-direction) for different incident optical power (P_{opt}) of wavelength λ = 700 nm are shown in Figs. 7 (a) and (b) (OW size: L_w = 0.20 μm, D_w = 0.40 mm, illumination area $A_w = L_w D_w = 0.80\times10^{-10}$ m^2). It can be observed from Figs. 7 (a) and (b) that the hole and electron dominated photocurrent densities are maximum when the light is incident entirely on n- and p-drift layers respectively. Also the photocurrent densities are maximum at the surface, i.e. at y = 0 and decrease gradually along the y-direction due to the optical absorption in the semiconductor base material (Si). The effective junction area of the device may be calculated from Fig. 1(a) as $A_j \approx (2h_{n+} + 4W_n + L_{n+})D_w \approx 10^{-9}$ m^2, where the height and length of the n^+-layer are taken to be h_{n+} = 0.20 μm and L_{n+} = 0.30 μm respectively, again keeping in mind the technological feasibility.

4.1 Static Properties

Variations of breakdown voltage ($V_B^{(\lambda,i)}$) of the device with starting position of the OW ($x_{ws}{}^{(i)}(x)$) along the length of the depletion layer (x-direction) for incident optical power of P_{opt} = 50 mW of different are shown in Fig. 8. The breakdown voltage of the device under unilluminated or dark condition is also indicated in the said figure (V_B = 24.36 V). It is interesting to observe from Fig. 8 that the maximum changes in $V_B^{(\lambda,i)}$ may be achieved when the starting position of the OW ($x_{ws}{}^{(i)}(x)$) is in between 0.40 and 0.58 μm for any wavelength under consideration. This fact indicates that maximum change in $V_B^{(\lambda,i)}$ of the device is occurred when the entire OW is created over the p-drift region, i.e. when the generated photocurrent is purely electron dominated. It is also noteworthy from Fig. 8 that the sensitivity of breakdown voltage is maximum for the 700 nm wavelength of the incident light which is very close to the wavelength corresponding to the peak responsivity of Si (i.e. λ = 750 nm).

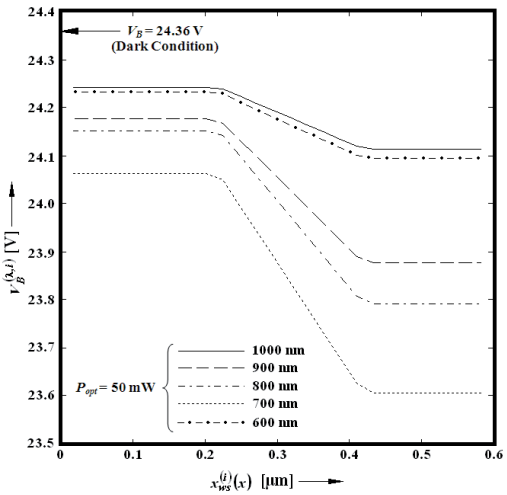

Fig. 8. Variations of breakdown voltage of lateral IMPATT device designed to operate at W-band with starting position of the OW along the length of the depletion layer (x-direction) for incident optical power of 50 mW of different wavelengths (OW size: L_w = 0.20 μm, D_w = 0.40 mm).

2-D static electric field and potential profiles of lateral DDR Si IMPATT device designed to operate at W-band under dark condition, illuminated conditions such as optical illumination over n-drift layer (OW position: x_{ws} =

0.10 μm, x_{we} = 0.30 μm; OW size: L_w = 0.20 μm, D_w = 0.40 mm) and optical illumination over on *p*-drift layer (OW position: x_{ws} = 0.50 μm, x_{we} = 0.70 μm; OW size: L_w = 0.20 μm, D_w = 0.40 mm) for incident optical power of 10 mW, 30 mW and 50 mW of wavelength of 700 nm are shown in Figs. 9 (a)–(g) and 10(a)–(g). It is observed from the above mentioned figures that, asymmetry and distortion are introduced in both 2-D static electric field and potential profiles of the device due to optical illumination. It is interesting to note that, the said asymmetry and distortion in static electric field and potential profiles of the device are more pronounced when the light is incident on *p*-drift layer, i.e. when the photocurrent is purely electron dominated.

Variations of breakdown voltage of the device with incident optical power of different wavelengths are shown in Fig. 11(a), for two different optical illumination configurations, such as (i) light is illuminated on *n*-drift layer, i.e. photocurrent is purely hole dominated (OW position: x_{ws} = 0.10 μm, x_{we} = 0.30 μm; OW size: L_w = 0.20 μm, D_w = 0.40 mm) and (ii) light is illuminated on *p*-drift layer, i.e. photocurrent is purely electron dominated (OW position: x_{ws} = 0.50 μm, x_{we} = 0.70 μm; OW size: L_w = 0.20 μm, D_w = 0.40 mm). It is observed from Fig. 11(a) that the breakdown voltage of the device decreases as the incident optical power is increased. Fig. 11(b) shows the variations of breakdown voltage of the device with wavelength of incident optical power of 50 mW, again for two different optical illumination configurations mentioned above. It can be reconfirmed from Figs. 11(a) and (b) that the breakdown voltage of the device is more sensitive to the electron dominated photocurrent as compared to its hole dominated counterpart. And also the 700 nm wavelength is found to be the most favorable wavelength to cause maximum modulation in breakdown voltage due to optical illumination.

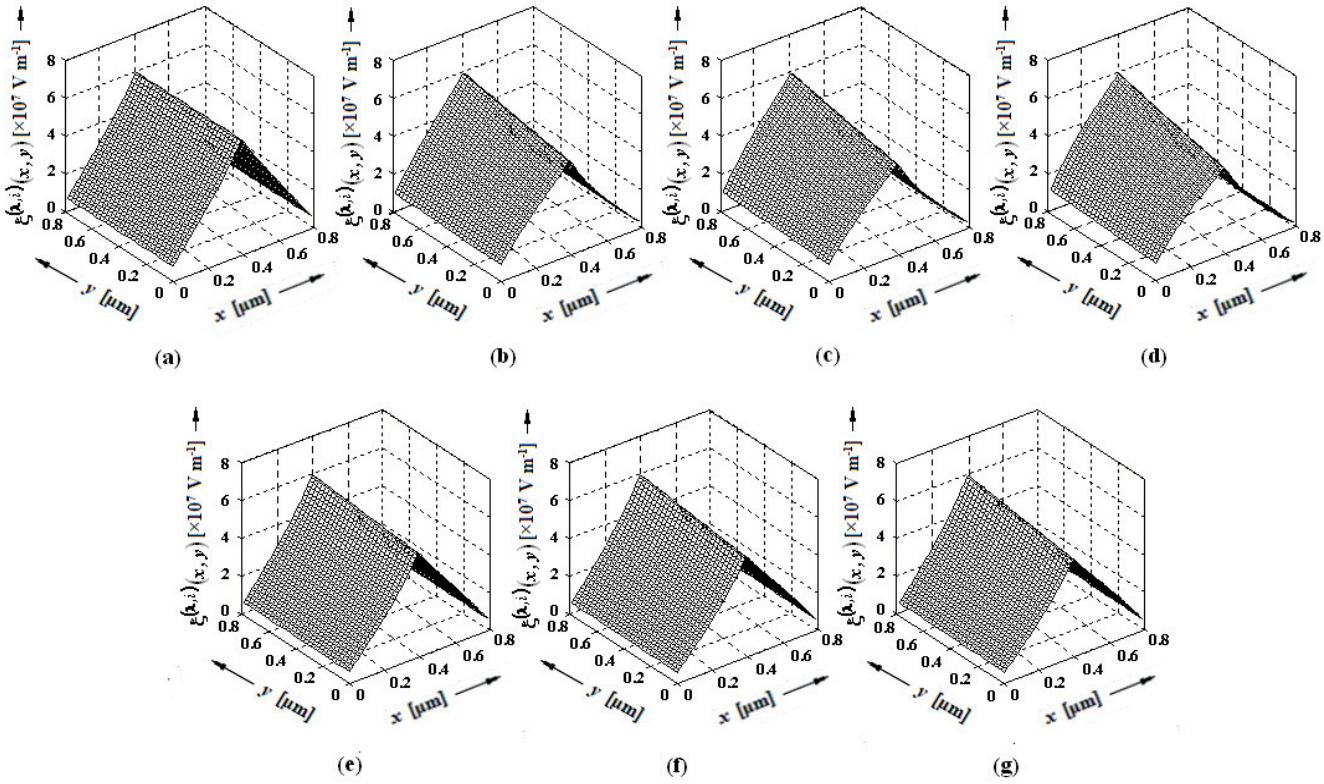

Fig. 9. 2-D static electric field profiles of lateral DDR Si IMPATT device designed to operate at W-band under **(a)** dark condition (P_{opt} = 0), illuminated condition for incident optical power of **(b)** P_{opt} = 10 mW, **(c)** P_{opt} = 30 mW, **(d)** P_{opt} = 50 mW of wavelength λ = 700 nm on *n*-drift layer (OW position: x_{ws} = 0.10 μm, x_{we} = 0.30 μm; OW size: L_w = 0.20 μm, D_w = 0.40 mm) and illuminated condition for incident optical power of **(e)** P_{opt} = 10 mW, **(f)** P_{opt} = 30 mW, **(g)** P_{opt} = 50 mW of wavelength λ = 700 nm on *p*-drift layer (OW position: x_{ws} = 0.50 μm, x_{we} = 0.70 μm; OW size: L_w = 0.20 μm, D_w = 0.40 mm) (2-D FDM: 70×70 grids).

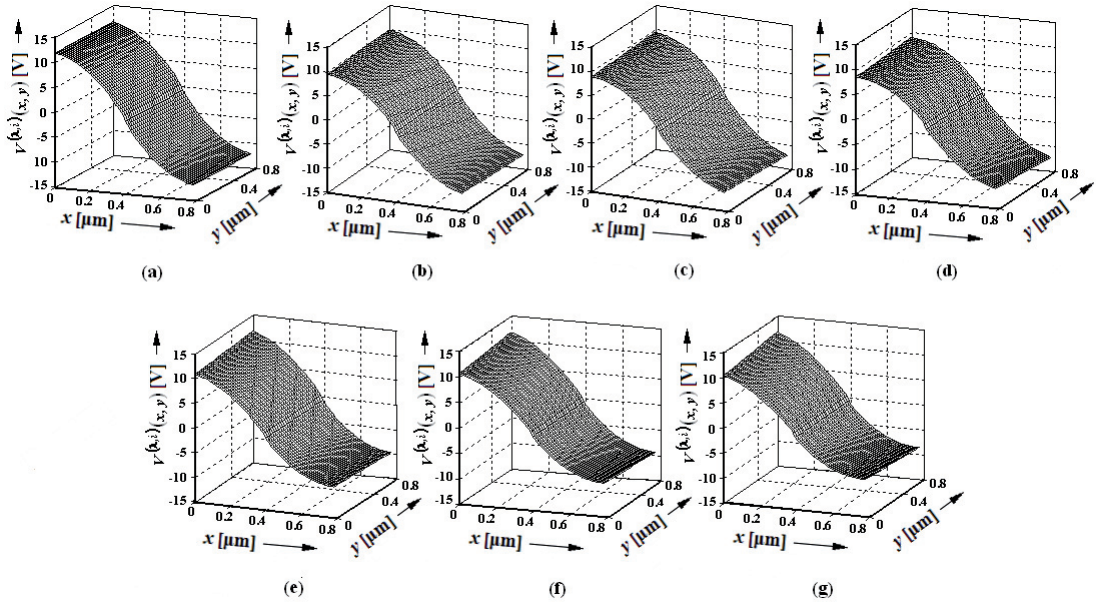

Fig. 10. 2-D static potential profiles of lateral DDR Si IMPATT device designed to operate at W-band under **(a)** dark condition (P_{opt} = 0), illuminated condition for incident optical power of **(b)** P_{opt} = 10 mW, **(c)** P_{opt} = 30 mW, **(d)** P_{opt} = 50 mW of wavelength λ = 700 nm on *n*-drift layer, i.e. due to hole dominated photocurrent (OW position: x_{ws} = 0.10 μm, x_{we} = 0.30 μm; OW size: L_w = 0.20 μm, D_w = 0.40 mm) and illuminated condition for incident optical power of **(e)** P_{opt} = 10 mW, **(f)** P_{opt} = 30 mW, **(g)** P_{opt} = 50 mW of wavelength λ = 700 nm on *p*-drift layer, i.e. due to electron dominated photocurrent (OW position: x_{ws} = 0.50 μm, x_{we} = 0.70 μm; OW size: L_w = 0.20 μm, D_w = 0.40 mm) (2-D FDM: 70×70 grids).

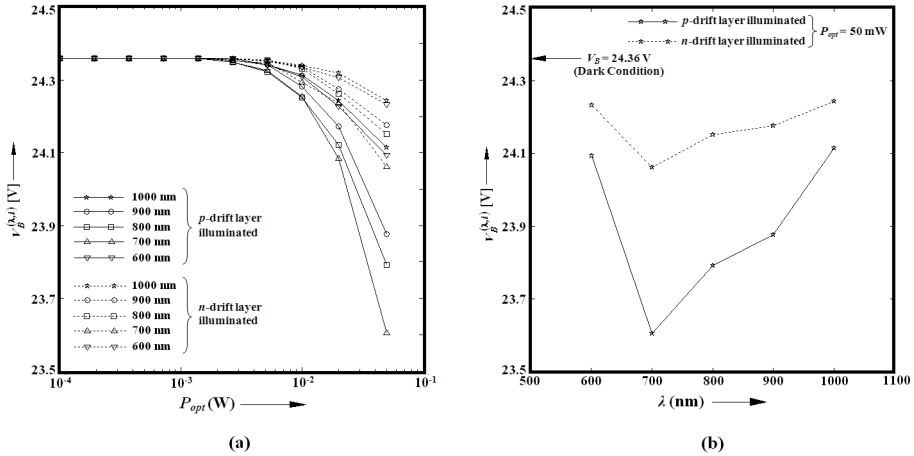

Fig. 11. Variations of breakdown voltage of lateral DDR Si IMPATT device designed to operate at W-band with **(a)** incident optical power of different wavelengths and with **(b)** wavelength for P_{opt} = 50 mW; for both the cases, light is illuminated on the *n*-drift layer (OW position: x_{ws} = 0.10 μm, x_{we} = 0.30 μm; OW size: L_w = 0.20 μm, D_w = 0.40 mm) and on the *p*-drift layer (OW position: x_{ws} = 0.50 μm, x_{we} = 0.70 μm; OW size: L_w = 0.20 μm, D_w = 0.40 mm).

4.2 L-S Properties

The L-S terminal voltage waveforms for voltage modulation factor of 50% and corresponding current responses at the metallurgical junction (i.e. at $x = x_j$) along the depth of the depletion layer (*y*-direction) under dark and both types of optical illumination configurations are shown in Figs. 12(a)–(f). Both voltage and current waveform get slightly distorted especially near the surface (i.e. at $y = 0$) due to the optical illumination. It is interesting to note from the figures that the above said distortions in terminal voltage and current waveforms are more prominent when light is incident on *p*-drift layer (Figs. 12(c) and (f)) as compared to when light is incident on *n*-drift layer (Figs. 12(b) and (e)).

Magnitudes of the real and imaginary parts of the device impedance under dark and two different optical illumination configurations (P_{opt} = 50 mW, λ = 700 nm) such as (i) light incident on *n*-drift layer (OW position: x_{ws} = 0.10 μm, x_{we} = 0.30 μm) and (ii) light incident on *p*-drift layer (OW position: x_{ws} = 0.50 μm, x_{we} = 0.70 μm) are plotted against frequency and shown in Figs. 13(a) and (b) respectively. OW size is kept fixed, i.e. L_w = 0.20 μm, D_w = 0.40 mm. It is observed that both the real and imaginary parts of the device impedance decrease due to the optical

illumination. The said decrease is more pronounced when the light is incident on the *n*-drift layer, i.e. due to purely electron dominated photocurrent. The avalanche resonance frequency at which the real part of the device impedance changes sign from positive to negative, is found to be f_a = 69.50 GHz under unilluminated or dark condition. But it is interesting to observe that, the avalanche resonance frequency of the device increases due to the optical illumination. The value of avalanche resonance frequency increases to 71.34 and 72.87 GHz when the optical power of 50 mW of wavelength 700 nm is allowed to incident entirely on *n*- and *p*-drift layers respectively. Thus the avalanche resonance frequency is also more sensitive to the purely electron dominated photocurrent as compared to its hole dominated counterpart. Admittance characteristics of the device are shown in Fig. 13(c) for dark and above mentioned optical illumination conditions. It is interesting to observe from Fig. 13(c) that the optimum frequency of the device for which the magnitude of negative conductance is maximum, increase due to the optical illumination. The optimum frequencies of the device are found to be 106.59 and 107.84 GHz when the optical power of 50 mW of wavelength 700 nm is allowed to incident entirely on *n*- and *p*-drift layers respectively; while the same is found to be 104.90 GHz under dark condition. The *Q*-factor of the device is an indicator of oscillation growth rate and stability of the source. Smaller the *Q*-factor, closer to one ($Q_p^{(\lambda,i)} \approx 1$), better the oscillation growth rate and stability. The *Q*-factor of the device is also observed to be increased due to the optical illumination which leads to deterioration in oscillation growth rate and stability. Greater degradation of *Q*-factor is observed due to purely electron dominated photocurrent.

Variations of peak negative conductance, RF power output, DC to RF conversion efficiency and optimum frequency of lateral IMPATT device designed to operate at W-band with starting positions of the optical window along the length of the depletion layer (*x*-direction) for incident optical power of 50 mW of different wavelengths are shown in Figs. 14(a), (b), (c) and (d) respectively. The OW size is kept fixed, i.e. L_w = 0.20 μm, D_w = 0.40 mm. It is interesting to observe from Figs. 14(a) – (d) that maximum changes in the above mentioned L-S parameters of the device due to optical illumination are occurred when the light is incident completely on the *p*-drift layer (i.e. when $x_{ws}^{(i)}(x) \geq x_j$ = 0.40 μm), i.e. when the generated photocurrent is purely electron dominated. Thus it may be concluded that, the OW has to be created over the *p*-drift layer to achieve the maximum optical modulation of the L-S properties of lateral DDR Si IMPATTs. Also the photosensitivity of the L-S properties of the device are found to be maximum at 700 nm wavelength, near the wavelength corresponding to the peak responsivity of Si (i.e. 750 nm).

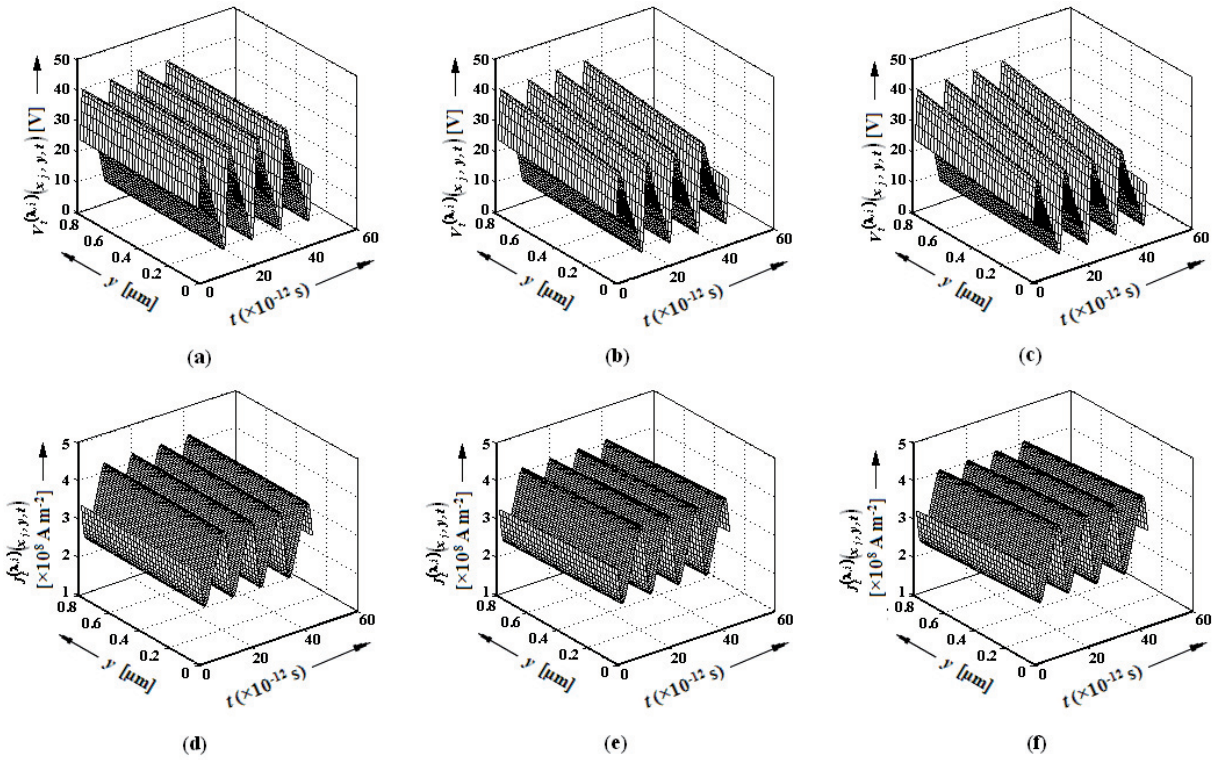

Fig. 12. The L-S terminal voltage waveforms for voltage modulation factor of 50% and corresponding current responses at the metallurgical junction (i.e. at $x = x_j$) along the depth of the depletion layer (*y*-direction); terminal voltage and current waveforms for **(a, d)** dark condition (P_{opt} = 0) and illuminated condition for incident optical power of 50 mW of wavelength 700 nm, when light is illuminated on **(b, e)** *n*-drift layer (purely hole dominated photocurrent; OW position: x_{ws} = 0.10 μm, x_{we} = 0.30 μm; OW size: L_w = 0.20 μm, D_w = 0.40 mm) and **(c, f)** *p*-drift layer (electron dominated photocurrent; OW position: x_{ws} = 0.50 μm, x_{we} = 0.70 μm; OW size: L_w = 0.20 μm, D_w = 0.40 mm).

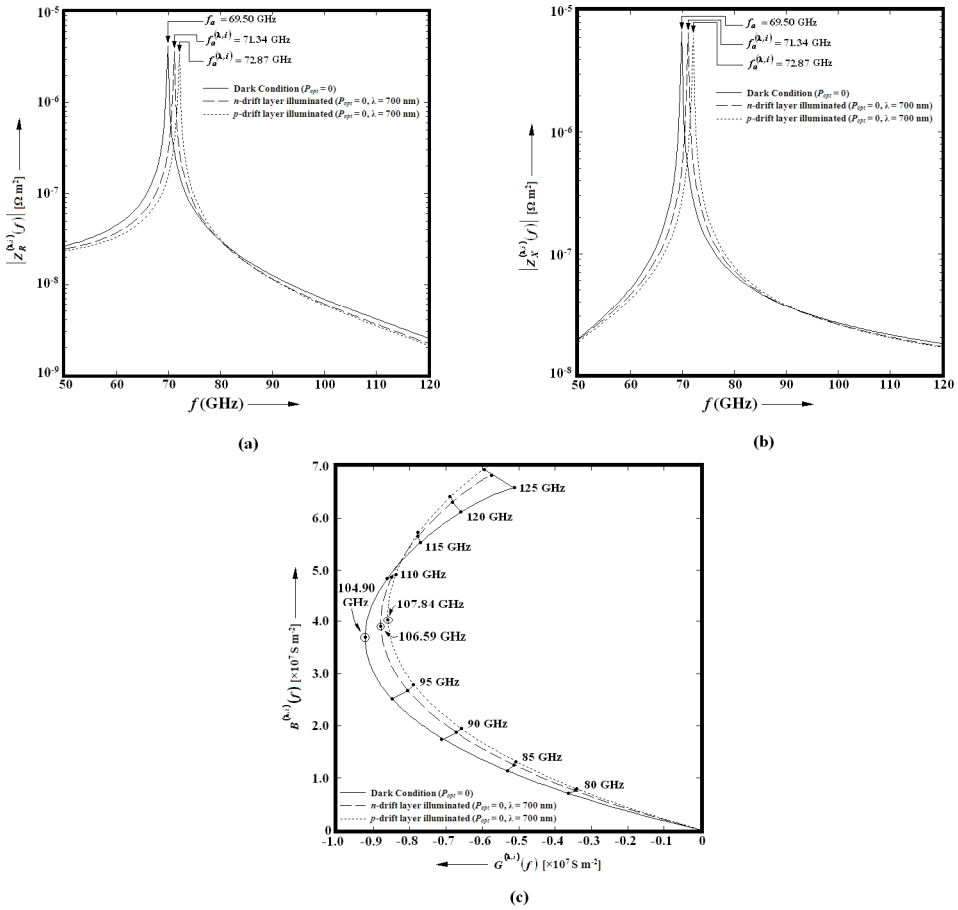

Fig. 13. Magnitudes of the **(a)** real and **(b)** imaginary parts of the device impedance vs. frequency plots and **(c)** admittance characteristics of the device under dark and two different optical illumination configuration (P_{opt} = 50 mW, λ = 700 nm) such as (i) light incident entirely on *n*-drift layer (OW position: x_{ws} = 0.10 μm, x_{we} = 0.30 μm; OW size: L_w = 0.20 μm, D_w = 0.40 mm) and (ii) light incident entirely on *p*-drift layer (OW position: x_{ws} = 0.50 μm, x_{we} = 0.70 μm; OW size: L_w = 0.20 μm, D_w = 0.40 mm).

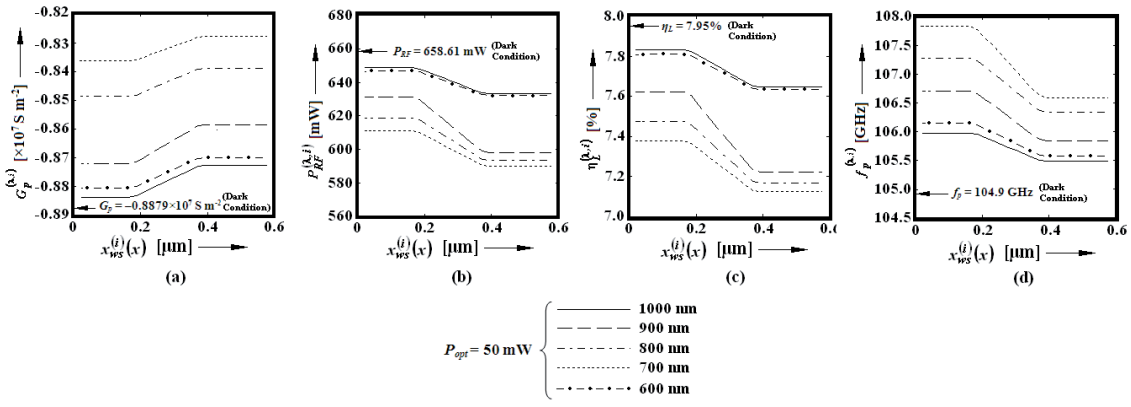

Fig. 14. Variations of **(a)** peak negative conductance, **(b)** RF power output, **(c)** DC to RF conversion efficiency and **(d)** optimum frequency of lateral IMPATT device designed to operate at W-band with starting positions of the optical window along the length of the depletion layer (*x*-direction) for optical power input of 50 mW of different wavelengths (OW size: L_w = 0.20 μm, D_w = 0.40 mm).

4.3 Validation of Simulation Results

Experimental results of optically illuminated conventional vertically oriented SDR Si IMPATTs show that the electron dominated photo current is more important than the hole dominated photocurrent in modulating the DC and RF properties of the device [19]. Simulation results presented in the present paper for optically illuminated lateral DDR Si IMPATT device exhibit a similar behavior as that observed experimentally in case of vertical SDR Si IMPATTs. The frequency tuning of IMPATT oscillators has also been experimentally demonstrated up to W-band by Seeds et al. [20], [21]. They observed a frequency tuning of 9.4 MHz for an SDR Si IMPATT oscillator operat-

ing at 91.83 GHz due to the optical illumination of 850 nm wavelength (GaAs/GaAlAs laser was used as the light source; a 50/125 μm graded index optical fiber was used to couple the light into the device) in which the electron dominated photocurrent (Top Mount configuration) was measured to be 20.3 μA. Whereas the present work shows that much more frequency tuning is achievable if the orientation of the DDR Si IMPATT device is chosen to be lateral instead of vertical. Also the 700 nm wavelength is found to be the most favorable wavelength for obtaining maximum optical modulation of L-S properties of the device.

But so far as authors' knowledge is concerned, no experimental report is available in published literature verifying the optical modulation of RF properties of lateral DDR Si IMPATTs. That is why, the simulation results could not be compared and validated with experimentally obtained data. But the experimental confirmation can be obtained by fabricating a number of W-band lateral DDR IMPATT device based on Si by using standard CMOS technology. The design parameters presented in this paper will be useful for this purpose. The OW of different devices may be created at different positions on the respective SiO_2 oxide layers by suitable photolithography and selective etching techniques. Finally measurement of the static and high frequency parameters of those devices may be carried out under both dark condition and also by coupling light energy of appropriate wavelength (600 to 1000 nm) over the different positions of the active region of the device. This study will provide the optical modulation characteristics of the device for different OW positions. The 3900S CW Tunable Ti:Sapphire Laser [22], [23] which is tunable within the wavelength range under consideration may be used as the optical source for the proposed experiment.

5. Conclusion

The optimum position of the optical window has been determined for which the finest optical control of high frequency properties of the lateral DDR Si IMPATT device can be achieved. A 2-D NSVE L-S simulation method has been developed by the authors for the illuminated lateral DDR IMPATTs. Simulation is carried out to study the optical modulation characteristics of the device for different incident optical power levels of different wavelengths by varying the position of the fixed sized OW along the electrical conduction axis of the device. Results show that the most favorable optical tuning of the RF properties of the device may be achieved when the optical window is entirely created over the *p*-type depletion layer, i.e. when the photocurrent is purely electron dominated. Also the 700 nm wavelength is found to be most suitable for obtaining maximum optical modulation of both DC and RF properties of the device.

Appendix I: List of Symbols

Symbol	Meaning
A_j	Effective junction area
A_W	Area of the optical window
$\alpha(\lambda)$	Absorption coefficient of semiconductor material at wavelength λ
$a_{n,p}$	Ionization coefficients of electrons or holes
$\alpha_n^{(\lambda,i)}(x,y,t)$	Ionization rate of electrons at the space point (x,y) at the instant of time t for optical illumination of wavelength λ and for i^{th} position of the optical window
$\alpha_p^{(\lambda,i)}(x,y,t)$	Ionization rate of holes at the space point (x,y) at the instant of time t for optical illumination of wavelength λ and for i^{th} position of the optical window
$B^{(\lambda,i)}(f)$	Susceptance of the diode at frequency f for optical illumination of wavelength λ and for i^{th} position of the optical window
$B_p^{(\lambda,i)}$	Susceptance of the diode corresponding to the optimum frequency for optical illumination of wavelength λ and for i^{th} position of the optical window
c	Velocity of light in free space ($c = 3.0\times10^8$ m s^{-1})
D	Impurity diffusion constant
$D_{n,p}$	Diffusion constant of electrons or holes
D_W	Width of the optical window
E	Measure of energy from the bottom of the conduction band on the *n*-side
E_g	Bandgap of the semiconductor material
$\xi^{(\lambda,i)}(x,y)$	DC electric field at the space point (x,y) for optical illumination of wavelength λ and for i^{th} position of the optical window
$\xi^{(\lambda,i)}(x,y,t)$	Time varying electric field at the space point (x,y) at the instant of time t for optical illumination of wavelength λ and for i^{th} position of the optical window
ε_s	Permittivity of the semiconductor material
f	Frequency
$f_a^{(\lambda,i)}$	Avalanche resonance frequency for optical illumination of wavelength λ and for i^{th} position of the optical window
f_d	Design frequency
$f_p^{(\lambda,i)}$	Optimum frequency for optical illumination of wavelength λ and for i^{th} position of the optical window
$G_{Ah^+}^{(\lambda,i)}(x,y,t)$	Avalanche generation rates of electrons at the space point (x,y) at the instant of time t for optical illumination of wavelength λ and for i^{th} position of the optical window
$G_{Ae^-}^{(\lambda,i)}(x,y,t)$	Avalanche generation rates of holes at the space point (x,y) at the instant of time t for optical illumination of wavelength λ and for i^{th} position of the optical window
$G^{(\lambda,i)}(f)$	Negative conductance of the diode at frequency f for optical illumination of wavelength λ and for i^{th} position of the optical window
$G_L^{(\lambda)}(y)$	EHP generation rate as a function of y for optical illumination of wavelength λ
$G_p^{(\lambda,i)}$	Negative conductance of the diode corresponding to the optimum frequency for optical illumination of wavelength λ and for i^{th} position of the optical window
$G_{Th^+}^{(\lambda,i)}(x,y,t)$	Tunneling generation rates of electrons at the space point (x,y) at the instant of time t for optical illumination of wavelength λ and for i^{th} position of the optical window
$G_{Te^-}^{(\lambda,i)}(x,y,t)$	Tunneling generation rates of holes at the space point (x,y) at the instant of time t for optical illumination of wavelength λ and for i^{th} position of the optical window
h	Planck's constant ($h = 6.625\times10^{-34}$ J s)
$\hbar$	Normalized Planck's constant ($\hbar = h/2\pi$)
J_0	DC bias current density
$J_{h^+(opt\_drt)}^{(\lambda,i)}(x,y$	Drift component of hole dominated photocurrent density holes at the space point (x,y) for optical illumination of

wavelength λ and for i^{th} position of the optical window

$J_{e^-(opt\_drt)}^{(\lambda,i)}(x,y)$ Drift component of electron dominated photocurrent density holes at the space point (x,y) for optical illumination of wavelength λ and for i^{th} position of the optical window

$J_{h^+(opt\_dff)}^{(\lambda,i)}(y)$ Drift component of hole dominated photocurrent density holes as a function of y for optical illumination of wavelength λ and for i^{th} position of the optical window

$J_{e^-(opt\_dff)}^{(\lambda,i)}(y)$ Drift component of electron dominated photocurrent density holes as a function of y for optical illumination of wavelength λ and for i^{th} position of the optical window

$J_{h^+(opt)}^{(\lambda,i)}(x,y)$ Total hole dominated photocurrent density at the space point (x,y) for optical illumination of wavelength λ and for i^{th} position of the optical window

$J_{e^-(opt)}^{(\lambda,i)}(x,y)$ Total electron dominated photocurrent density at the space point (x,y) for optical illumination of wavelength λ and for i^{th} position of the optical window

$J_{h^+(tot)}^{(\lambda,i)}(x,y,t)$ Total hole component of current density at the space point (x,y) at the instant of time t for optical illumination of wavelength λ and for i^{th} position of the optical window

$J_{e^-(tot)}^{(\lambda,i)}(x,y,t)$ Total electron component of current density at the space point (x,y) at the instant of time t for optical illumination of wavelength λ and for i^{th} position of the optical window

$L_{n,p}$ Diffusion lengths of electrons or holes

L_W Length of the optical window

$l_n^{(i)}(x)$ Effective length of the optical window over the n-epitaxial layers

$l_p^{(i)}(x)$ Effective length of the optical window over the p-epitaxial layers

λ Wavelength

$\lambda_n(x)$ Parameter related to the doping profile of n-epitaxial layer

$\lambda_p(x)$ Parameter related to the doping profile of p-epitaxial layer

m_d^* Density of state effective mass of charge carriers

$m_{n,p}$ Constants associated with ionization rates of electrons or holes

m_n^* Effective mass of electrons in conduction band

m_p^* Effective mass of holes in valance band

m_x Voltage modulation factor

$\mu_{n,p}$ Mobility of electrons or holes

N_A Acceptor concentration of p-epitaxial layer

N_c Effective density of states of conduction band

N_D Donor concentration of n-epitaxial layer

N_v Effective density of states of valance band

N_{n+} Donor concentration of n^+-highly doped layer

N_{p+} Acceptor concentration of p^+-highly doped layer

$N(x,y)$ Doping concentration at the space point (x,y)

n_i Intrinsic carrier concentration

$n_a(\lambda)$ Refractive index of air at wavelength λ

$n_s(\lambda)$ Refractive index of semiconductor material at wavelength λ

$n_{int}(\lambda)$ Internal quantum efficiency of semiconductor material at wavelength λ

$n^{(\lambda,i)}(x,y,t)$ Electron concentration at the space point (x,y) at the instant of time t for optical illumination of wavelength λ and for i^{th} position of the optical window

$\eta_L^{(\lambda,i)}$ DC to RF conversion efficiency for optical illumination of wavelength λ and for i^{th} position of the optical window

$P^{(\lambda,i)}(x,y,t)$ Normalized current density at the space point (x,y) for optical illumination of wavelength λ and for i^{th} position of the optical window

$P_{DC}^{(\lambda,i)}$ DC input power for optical illumination of wavelength λ and for i^{th} position of the optical window

P_{opt} Optical power input

$P_{RF}^{(\lambda,i)}$ RF power output for optical illumination of wavelength λ and for i^{th} position of the optical window

$p^{(\lambda,i)}(x,y,t)$ Hole concentration at the space point (x,y) at the instant of time t for optical illumination of wavelength λ and for i^{th} position of the optical window

$\Phi_0(\lambda)$ Surface density of the photon flux optical illumination of wavelength λ

q Electric charge of an electron ($q = 1.6\times10^{-19}$ C)

$Q_p^{(\lambda,i)}$ Quality factor corresponding to the optimum frequency for optical illumination of wavelength λ and for i^{th} position of the optical window

$R'(\lambda)$ Reflectance of the semiconductor-air interface for optical illumination of wavelength λ

t Any time instant

T_d Time period corresponding to the design frequency

t_d Time for diffusion

T_j Junction temperature

VB DC breakdown voltage under dark condition

$V_B^{(\lambda,i)}$ DC breakdown voltage for optical illumination of wavelength λ and for i^{th} position of the optical window

$V^{(\lambda,i)}(x,y)$ DC electric potential at the space point (x,y) for optical illumination of wavelength λ and for i^{th} position of the optical window

$V^{(\lambda,i)}(x,y,t)$ Electric potential at the space point (x,y) at the instant of time t for optical illumination of wavelength λ and for i^{th} position of the optical window

$v_n^{(\lambda,i)}(x,y,t)$ Drift velocity of at the space point (x,y) for optical illumination of wavelength λ and for i^{th} position of the optical window

$v_p^{(\lambda,i)}(x,y,t)$ Drift velocity of holes at the space point (x,y) for optical illumination of wavelength λ and for i^{th} position of the optical window

$v_{rf}(t)$ Non-sinusoidal RF voltage

V_{RF1} Amplitude of the fundamental component of the RF voltage

$V_t^{(\lambda,i)}(t)$ Instantaneous diode terminal voltage for optical illumination of wavelength λ and for i^{th} position of the optical window

W Total depletion layer width ($W = W_n + W_p$)

W_n n-epitaxial layer width

W_p p- epitaxial layer width

W_{n+} n^+-contact layer width

W_{p+} p^+-contact layer width

x x-coordinate

x_1 x-coordinate on n-epitaxial layer near the metallurgical junction

x_2 x-coordinate on p-epitaxial layer near the metallurgical junction

x_j x-coordinate of the metallurgical junction

x_{we0} Initial ending position of the optical window

x_{ws0} Initial starting position of the optical window

x_{wsf} Final starting position of the optical window

$x_{we}^{(i)}(x)$ Coordinate of the ending edge of the optical window

$x_{ws}^{(i)}(x)$ Coordinate of the starting edge of the optical window

Δx Space length per shift of the optical window position

y y-coordinate

$Y_D^{(\lambda,i)}(f)$ L-S admittance of IMPATT diode for frequency f for optical illumination of wavelength λ and for i^{th} position of the optical window

$Z_R^{(\lambda,i)}(f)$ L-S negative resistance of IMPATT diode for frequency f for optical illumination of wavelength λ and for i^{th} position of the optical window

$Z_X^{(\lambda,i)}(f)$ L-S reactance of IMPATT diode for frequency f for optical illumination of wavelength λ and for i^{th} position of the optical window

Acknowledgement

The senior most author, Professor (Dr.) J. P. Banerjee (same as J. P. Bandyopadhyay) is grateful to the University Grants Commission, India for supporting the research through the award of an Emeritus Fellowship in the Inst. of Radio Physics and Electronics, University of Calcutta.

References

[1] STABILE, P. J., LALEVIC, B. Lateral IMPATT diodes. *IEEE Trans. on Electron devices*, 1989, vol. 10, no. 6, p. 249-251.

[2] AL-ATTAR, T., LEE, T. H. Monolithic integrated millimeter-wave IMPATT transmitter in standard CMOS technology. *IEEE Trans. on MTT*, 2005, vol. 53, no. 11, p. 3557-3561.

[3] AL-ATTAR, T. CMOS diodes operating beyond avalanche frequency. In *12th Int. Symp. on Quality Electronic Design (ISQED)*. March 14-16, 2011, p. 1-6.

[4] ACHARYYA, A., BANERJEE, J. P. A proposed lateral DDR IMPATT structure for better millimeter-wave optical interaction. In *IEEE International Conference on Devices, Circuits and Systems.* Coimbatore, Tamil Nadu, 15-16 March 2012, p. 599-602.

[5] ACHARYYA, A., BANERJEE, B., BANERJEE, J. P. Optical control of millimeter-wave lateral double-drift region silicon IMPATT device. *Radioengineering*, 2012, vol. 21, no. 4, p. 1208–1217.

[6] SZE, S. M., RYDER, R. M. Microwave avalanche diodes. *Proc. of IEEE*, *Special Issue on Microwave Semiconductor Devices*, 1971, vol. 59, no. 8, p. 1140-1154.

[7] ACHARYYA, A., CHAKRABORTY, J., DAS, K., DATTA, S., DE, P., BANERJEE, S., BANERJEE, J. P. Large-signal characterization of DDR silicon IMPATTs operating up to 0.5 THz. *International Journal of Microwave and Wireless Technologies*, vol. 5, no. 5, p. 567-578.

[8] STUPELMAN, V., FILARETOV, G. *Semiconductor Devices*. Moscow: Mir Publications,1976.

[9] GRANT, W. N. Electron and hole ionization rates in epitaxial silicon. *Solid State Electron*, 1973, vol. 16, no. 10, p. 1189-1203.

[10] CANALI, C., OTTAVIANI, G., QUARANTA, A. A. Drift velocity of electrons and holes and associated anisotropic effects in silicon. *J. Phys. Chem. Solids*, 1971, vol. 32, no. 8, p. 1707.

[11] Electronic Archive: New Semiconductor Materials, Characteristics and Properties, 2013. [Online] Available at: http://www.ioffe.ru/SVA/NSM/Semicond/Si/index.html.

[12] VARSHNI, Y. P. Temperature dependence of the energy gap in semiconductors. *Physica*, 1967, vol. 34 p. 149-154.

[13] RAJKANAN, K., SINGH, R., SHEWCHUN, J. Absorption coefficient of silicon for solar cell calculations. *Solid-Sate Electron.*, 1979, vol. 22, p. 793-795.

[14] BUCHER, K., BRUNS, J., WAGEMANN, H. G. Absorption coefficient of silicon: An assessment of measurements and the simulation of temperature variation. *J. Appl. Phys.*, 1994, vol. 75, no. 2, p. 1127-1131.

[15] KANE, E. O. Theory of tunneling. *Journal of Applied Physics*, 1961, vol. 32, p. 83-91.

[16] ACHARYYA, A., CHAKRABORTY, J., DAS, K., DATTA, S., DE, P., BANERJEE, S., BANERJEE, J. P. Large-signal characterization of DDR silicon IMPATTs operating in millimeter-wave and terahertz regime. *Journal of Semiconductors*, 2013, vol. 34, no. 10, p. 104003-8.

[17] ACHARYYA, A., MUKHERJEE, M., BANERJEE, J. P. Effects of tunneling current on mm-wave IMPATT devices. *International Journal of Electronics*, 2013, in press.

[18] KURATA, M. *Numerical Analysis for Semiconductor Devices.* Lexington MA: Heath, 1982.

[19] VYAS, H. P., GUTMANN, R. J., BORREGO, J. M. Effect of hole versus electron photocurrent on microwave-optical interactions in IMPATT oscillators. *IEEE Transactions on Electron Devices*, 1979, vol. 26, no. 3, p. 232-234.

[20] SEEDS, A. J., AUGUSTO, A. Optical control of microwave semiconductor devices. *IEEE Trans. on Microwave Theory and Techniques*, 1990, vol. 38, no. 5, p. 577-585.

[21] SEEDS, A. J., SINGLETON, J. F., BRUNT, S. P., AUGUSTO, A. The optical control of IMPATT oscillators. *Journal of Lightwave Technology*, 1987, vol. 5, no. 3, p. 403-411.

[22] CW Tunable Ti:Sapphire Laser 3900S, 2013. Available at: http://www.newport.com/3900S-CW-Tunable-Ti-Sapphire-Laser/368139 /1033/info.aspx#tab_Specifications.

[23] ACHARYYA, A., BANERJEE, S., BANERJEE, J. P. Optical control of large-signal properties of millimeter-wave and sub-millimeter-wave DDR Si IMPATTs. *Journal Computational Electronics*, 2013, DOI 10.1007/s10825-013-0550-z.

About Authors ...

Aritra ACHARYYA was born in 1986. He received M. Tech. degree from the Institute of Radio Physics and Electronics, University of Calcutta, Kolkata, India in the year 2010. He is currently pursuing PhD work in the field of millimeter-wave and terahertz semiconductor devices and their optical control.

Jayabrata GOSWAMI was born in 1984. He received M. Tech degree from the Institute of Radio Physics and Electronics, University of Calcutta, Kolkata, India in the year 2010. He is carrying out PhD work in the field of quantum effect devices.

Suranjana BANERJEE was born in 1980. She received M. Tech. degree from the Institute of Radio Physics and Electronics, University of Calcutta, Kolkata, India. She has been carrying out research work in the area of both homo-junction and hetero-junction ATT devices under CW and pulsed operations at millimeter wave and terahertz frequency bands.

Professor (Dr.) J. P. BANERJEE (same as J. P. BANDYOPADHYAY) was born in 1947. He received the graduation and master degrees in Physics and PhD degree in Radio Physics and Electronics, all from the University of Calcutta. He was the reader in the Department of Electronic Science, C.U. from 1989 to 1998 and then full Professor in the Institute of Radio Physics and Electronics, C.U. from 1998 to 2012. He is presently an Emeritus Professor in the Institute of Radio Physics and Electronics, C.U., India. He is the principal co-author of more than 200 research papers in international journals in the fields of semiconductor science and technology, microwave, millimeter-wave and photonic devices.